

Bone Anisotropy – Analytical and Finite Element Analysis

Abstract

A human femur model, submitted to static loads, is analyzed through the utilization of three material constitutive relationships, namely: isotropic, transversally isotropic and orthotropic. The influence of bone anisotropy with respect to principal stress/strain distribution on human femur external surface was accessed through the use of analytical and finite element approaches. The models results show that the principal angles at a medial path bone surface have a good correlation with human femur bone lamellae angles.

Keywords

Bone anisotropy, principal stresses, principal strains, principal angles.

Lucas Lisboa Vignoli ^a

Paulo Pedro Kenedi ^b

^a Department of Mechanical Engineering, Pontifical Catholic University of Rio de Janeiro, Rua Marques de São Vicente 225 - Gavea, Rio de Janeiro, RJ - CEP 22453-900 - Brazil.

lucaslvig@gmail.com

^b PPEMM - Programa de Pós-Graduação em Engenharia Mecânica e Tecnologia de Materiais - CEFET/RJ - Av. Maracanã, 229 - Maracanã - RJ - CEP 20271-110 - Brazil.

paulo.kenedi@cefet-rj.br

<http://dx.doi.org/10.1590/1679-78251814>

Received 29.12.2014

In Revised Form 21.08.2015

Accepted 26.08.2015

Available online 22.09.2015

1 INTRODUCTION

Bone is a live tissue which is responsible for sustaining the human body. It can grow and self-repair. Bones are submitted to the action of the muscles loads and the gravity. Long bones, as femurs, for instance, provide stability and support for a person to remain standing or walking.

Many researches have been done in Biomechanics area. In order to position this paper along with the other bone anisotropy papers, a short overview of the Biomechanical works were provided, freely classifying them in different areas/approaches. Among the papers that deal with the bone anisotropy, there are those that describe the structural bone details. These papers are named here as **micro/nano** papers, as in Carnelli *et al.* (2013) and in Baumann *et al.* (2012).

Others papers only consider the macroscopic effects and are named here as **macro** papers, as it is this manuscript. There are papers that use Finite Element software to model bone, named here as **numerical** papers, as in Kenedi and Vignoli (2014), in San Antonio *et al.* (2012) like this manuscript. Other papers use theoretical/analytical methodologies, as mechanics of solids, theory of elasticity, homogenization theory and so on. These papers are named here as **analytical** papers, as in Toridis (1969) like this manuscript as well. Experimental approaches can be also used, through the utilization of sensors/transducers to measure diverse mechanical characteristics of bones, as for instance, to obtain better elastic material constants to describe such a complex material as bone. These papers are named here as **experimental** papers, as in Allena and Clusel (2014). Also there are papers that cover two or more areas; these papers are named here as **multi-area** papers.

This paper, *Bone Anisotropy - Analytical and Finite Element Analysis*, called for now on **actual** paper, is classified as a multi-area paper, which covers macro, analytical and numerical areas. The actual paper can be classified as a macro paper because it uses classical elastic material constants to describe a complex material as bones that although having a complex internal structure, only utilize the summation of their mechanical effects. It can also be considered an analytical paper because the actual paper uses the expressions obtained by theory of elasticity to describe the principal stress/strain distribution and correspondent principal angles at a medial external bone surface path. It can also be considered a numerical paper because it uses a finite element model as reference to the analytical one.

In this work, three constitutive relationships - orthotropic, transversally isotropic and isotropic - were used to estimate the principal stress/strain values and the correspondent principal angles, on a path at medial external surface of a human femur, with the objective of verify if the Petrář *et al.* (1996) and Cowin and Hart (1990) propositions that the principal stress angles at a medial external surface of a human femur were compatible with the dominant osteonal direction.

There are many examples of the theory of elasticity applied to isotropic materials, as for instance, in Sokolnikoff (1956). For anisotropic materials, some important contributions are found in Lekhnitskii (1981) for general theory of elasticity, which is used as basis for this present analytical model. As an improvement of the isotropic femur analytical stress analysis proposed by Kenedi and Riagusoff (2015) and of the FE analysis proposed by Kenedi and Vignoli (2014), this paper develops a stress and strain analysis of a human femur taking into account its natural anisotropy using expressions derived from the theory of elasticity Lekhnitskii (1981) and uses a FE software.

At next section, a short introduction to material anisotropy is presented, showing the differences between the especially important constitutive relations for this work: the isotropic, the transversally isotropic and the orthotropic.

2 MATERIAL ANISOTROPY

Bones, from a macroscopic point of view, can be classified as non-homogeneous, porous and anisotropic tissue, Doblaré *et al.* (2004). At a human femur cortical and trabecular bone tissues can coexist, although for the medial cross section analyzed in this work only cortical bone is present.

It is very difficult to obtain experimentally bone elastic mechanical properties. Some authors like Taylor *et al.* (2002) have obtained orthotropic bone elastic properties indirectly, through the utilization of modal analysis and Finite Element Method approaches. To overcome this difficulty authors like Jones (1998) and Krone and Schuster (2006) present different constitutive relationships to model bone behavior, among them, there are three constitutive relationships that are especially important for this work: the isotropic, the transversally isotropic and the orthotropic.

The isotropic materials have only two independent mechanical elastic constants, the Young modulus E and the Poisson ratio ν . The transversally isotropic materials have five independent mechanical elastic constants, two Young modulli, one shear modulus and two Poisson ratios. The orthotropic materials have nine independent mechanical elastic constants, three Young modulli, three shear modulli and three Poisson ratios, Jones (1998).

These mechanical elastic constants are placed at the stiffness matrix S , which relates stresses and strains. Hooke’s law can also be written in a different form using a compliance matrix C as

$$e_{jr} = C_{jrlm} \tau_{lm} \tag{1}$$

where e_{jr} are the strain components, C_{jrlm} are the compliance matrix components and τ_{lm} are the stress components. Note that e , C and τ are tensors.

The geometric compatibility and the equilibrium equations are represented, respectively, by equations (2) and (3)

$$e_{lm} = \frac{1}{2} \left(\frac{\partial u_l}{\partial x_m} + \frac{\partial u_m}{\partial x_l} \right) \tag{2}$$

$$\frac{\partial \tau_{ij}}{\partial x_j} + f_i = 0 \tag{3}$$

where u are the displacements, x are the coordinates and f are the body forces. Also note that these equations can be expanded according to the coordinate system.

At next section the analytical model is described in details. The principal stresses and principal strains expressions are explicitly presented as well as the correspondent principal angles.

3 ANALYTICAL MODEL

For anisotropic materials the matricial strain-stress relation is presented in equation (1). For orthotropic materials the compliance matrix can be simplified, as show explicitly in equation (4), Jones (1998):

$$C = \begin{bmatrix} \frac{1}{E_1} & -\frac{\nu_{21}}{E_2} & -\frac{\nu_{31}}{E_3} & 0 & 0 & 0 \\ -\frac{\nu_{12}}{E_1} & \frac{1}{E_2} & -\frac{\nu_{32}}{E_3} & 0 & 0 & 0 \\ -\frac{\nu_{13}}{E_1} & -\frac{\nu_{23}}{E_2} & \frac{1}{E_3} & 0 & 0 & 0 \\ 0 & 0 & 0 & \frac{1}{G_{23}} & 0 & 0 \\ 0 & 0 & 0 & 0 & \frac{1}{G_{13}} & 0 \\ 0 & 0 & 0 & 0 & 0 & \frac{1}{G_{12}} \end{bmatrix} \tag{4}$$

Where, E_1 , E_2 and E_3 are, respectively, the Young modulli on directions 1, 2 and 3; G_{12} , G_{13} and G_{23} are, respectively, the shear modulli; ν_{12} , ν_{13} , ν_{21} , ν_{23} , ν_{31} and ν_{32} are Poisson ratios. Note that to ensure the matrix symmetry, the condition $(\nu_{ij}/E_i) = (\nu_{ji}/E_j)$ must be satisfied.

As mentioned previously, nine constants are necessary to characterize an orthotropic material, five for a transversally isotropic and just two for an isotropic material. The transversally isotropic material is a special case of orthotropy, where the material is isotropic along the cross section, thus its independent constants are $E_1 = E_2, E_3, \nu_{23} = \nu_{13}, \nu_{12}$ and $G_{23} = G_{13}$. Note that $G_{12} = E_1/(1 + \nu_{12})$ is an independent property. Another form of representing matricial stress-strain relation is using stiffness components S , Jones (1998):

$$\tau_{jr} = S_{jr|lm} e_{lm} \quad (5)$$

The analytical model presented in this work, Lekhnitskii (1981), has the following hypotheses: the model is applied to a hollow cylindrical bone; the body is orthotropic with the properties defined by a cylindrical coordinate system, where the mechanical properties are constant along each direction. Note that the internal loads and moments at a medial cross section centroid are represented in a cartesian coordinate system. Figure 1 shows, at a medial cross section, the two coordinates system used in this manuscript: the cartesian and the cylindrical.

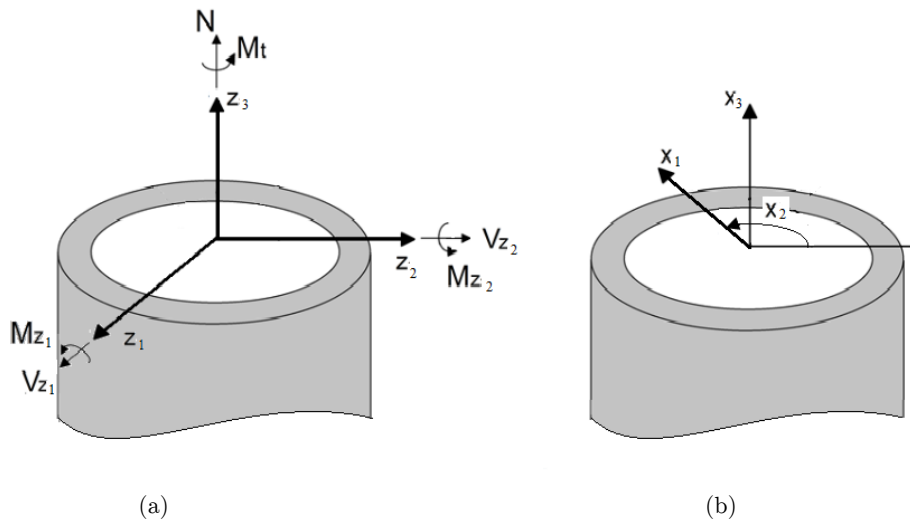


Figure 1: The coordinates systems at a medial cross-section:
(a) cartesian with forces and moments components and (b) cylindrical.

The internal loads and moments at a medial cross section centroid, represented at Fig. 1.a, can be obtained from the equivalent representation of the static loading positioned at the femur head region. See, for instance, the hollow circular bone model of Kenedi and Riagusoff (2015).

To get a solution for the stress and the strain field along the cylinder cross section, two stress functions, F and ψ , have to satisfy the following equations, Lekhnitskii (1981):

$$\tau_{11} = \frac{1}{x_1} \frac{\partial F}{\partial x_1} + \frac{1}{(x_1)^2} \frac{\partial^2 F}{\partial (x_2)^2} \tag{6.a}$$

$$\tau_{22} = \frac{\partial^2 F}{\partial (x_1)^2} \tag{6.b}$$

$$\tau_{12} = -\frac{\partial^2 F}{\partial x_1 \partial x_2} \left(\frac{F}{x_1} \right) \tag{6.c}$$

$$\tau_{13} = \frac{1}{x_1} \frac{\partial \psi}{\partial x_2} \tag{6.d}$$

$$\tau_{23} = -\frac{\partial \psi}{\partial x_1} \tag{6.e}$$

The stress τ_{33} can be related to the other stress components using geometric compatibility, presented in equation (2), or the identity, that can be verified by substitution, and is expressed in equation (7):

$$\left(\frac{\partial^2}{\partial (x_2)^2} - x_1 \frac{\partial}{\partial x_1} \right) e_{11} + x_1 \frac{\partial^2}{\partial (x_1)^2} (x_1 e_{22}) - \frac{\partial^2}{\partial x_1 \partial x_2} (x_1 e_{12}) = 0 \tag{7}$$

With these stress functions, the identity and the equations presented previously, namely constitutive, geometric compatibility and equilibrium; it is possible to propose the stress distribution for each load: axial, bending, torsional and transversal shear, through the implementation of the boundary conditions Lekhnitskii (1981).

The axial force N applied on the cylinder has a triaxial state of stress as shown in equation (8), where the radial normal stress must be zero on the free surface as there is no external pressure, Lekhnitskii (1981):

$$\tau_{11}^{axial} = \frac{N\hbar}{T} \left(1 - \frac{1-\rho^{k+1}}{1-\rho^{2k}} \left(\frac{x_1}{R_e} \right)^{k-1} - \frac{1-\rho^{k-1}}{1-\rho^{2k}} \rho^{k+1} \left(\frac{x_1}{R_e} \right)^{-k-1} \right) \tag{8.a}$$

$$\tau_{22}^{axial} = \frac{N\hbar}{T} \left(1 - \frac{1-\rho^{k+1}}{1-\rho^{2k}} k \left(\frac{x_1}{R_e} \right)^{k-1} + \frac{1-\rho^{k-1}}{1-\rho^{2k}} k \rho^{k+1} \left(\frac{x_1}{R_e} \right)^{-k-1} \right) \tag{8.b}$$

$$\tau_{33}^{axial} = \frac{N}{T} - \frac{N\hbar}{TC_{3333}} \left(C_{1133} + C_{2233} - \frac{1-\rho^{k+1}}{1-\rho^{2k}} (C_{1133} + kC_{2233}) \left(\frac{x_1}{R_e} \right)^{k-1} - \frac{1-\rho^{k-1}}{1-\rho^{2k}} (C_{1133} - kC_{2233}) \rho^{k+1} \left(\frac{x_1}{R_e} \right)^{-k-1} \right) \tag{8.c}$$

Where R_e is the external radius, R_i is the internal radius, $\rho = R_i/R_e$ is the ratio between the internal and the external radii.

At Appendix 1 it is defined the additional parameters h , T and k , that were created to get a more compact expression presentation. At Appendix 2 is shown the error that occurs if it is considered that the whole cross section has the same displacement, independent of the radial coordinates.

The stress distribution produced by the bending moment M in global coordinate z_1 are, Lekhnitskii (1981):

$$\tau_{11}^{bend-z1} = \frac{M_{z_1} R_e g}{K} \left[\left(\frac{x_1}{R_e} \right) - \left(\frac{1-\rho^{m+2}}{1-\rho^{2m}} \right) \left(\frac{x_1}{R_e} \right)^{m-1} - \left(\frac{1-\rho^{m-2}}{1-\rho^{2m}} \right) \rho^{m+2} \left(\frac{x_1}{R_e} \right)^{-m-1} \right] \sin(x_2) \quad (9.a)$$

$$\tau_{22}^{bend-z1} = \frac{M_{z_1} R_e g}{K} \left[3 \left(\frac{x_1}{R_e} \right) - \left(\frac{1-\rho^{m+2}}{1-\rho^{2m}} \right) (1+m) \left(\frac{x_1}{R_e} \right)^{m-1} - \left(\frac{1-\rho^{m-2}}{1-\rho^{2m}} \right) \rho^{m+2} (1-m) \left(\frac{x_1}{R_e} \right)^{-m-1} \right] \sin(x_2) \quad (9.b)$$

$$\tau_{33}^{bend-z1} = - \left\{ - \frac{M_{z_1}}{K} x_1 \sin(x_2) + \frac{M_{z_1} R_e g}{K C_{3333}} \left[(C_{1133} + 3C_{2233}) \left(\frac{x_1}{R_e} \right) - \left(\frac{1-\rho^{m+2}}{1-\rho^{2m}} \right) (C_{1133} + (1+m)C_{2233}) \left(\frac{x_1}{R_e} \right)^{m-1} - \left(\frac{1-\rho^{m-2}}{1-\rho^{2m}} \right) \rho^{m+2} (C_{1133} + (1-m)C_{2233}) \left(\frac{x_1}{R_e} \right)^{-m-1} \right] \right\} \sin(x_2) \quad (9.c)$$

$$\tau_{12}^{bend-z1} = - \frac{M_{z_1} R_e g}{K} \left[\left(\frac{x_1}{R_e} \right) - \left(\frac{1-\rho^{m+2}}{1-\rho^{2m}} \right) \left(\frac{x_1}{R_e} \right)^{m-1} - \left(\frac{1-\rho^{m-2}}{1-\rho^{2m}} \right) \rho^{m+2} \left(\frac{x_1}{R_e} \right)^{-m-1} \right] \cos(x_2) \quad (9.d)$$

Where m , g and K are additional parameters created to get more compact expressions and are defined at Appendix 1. For the bending moment M applied on the global coordinate z_2 the stress expressions are, Lekhnitskii (1981):

$$\tau_{11}^{bend-z2} = - \frac{M_{z_2} R_e g}{K} \left[\left(\frac{x_1}{R_e} \right) - \left(\frac{1-\rho^{m+2}}{1-\rho^{2m}} \right) \left(\frac{x_1}{R_e} \right)^{m-1} - \left(\frac{1-\rho^{m-2}}{1-\rho^{2m}} \right) \rho^{m+2} \left(\frac{x_1}{R_e} \right)^{-m-1} \right] \cos(x_2) \quad (10.a)$$

$$\tau_{22}^{bend-z2} = - \frac{M_{z_2} R_e g}{K} \left[3 \left(\frac{x_1}{R_e} \right) - \left(\frac{1-\rho^{m+2}}{1-\rho^{2m}} \right) (1+m) \left(\frac{x_1}{R_e} \right)^{m-1} - \left(\frac{1-\rho^{m-2}}{1-\rho^{2m}} \right) \rho^{m+2} (1-m) \left(\frac{x_1}{R_e} \right)^{-m-1} \right] \cos(x_2) \quad (10.b)$$

$$\tau_{33}^{bend-z2} = \left\{ - \frac{M_{z_2}}{K} x_1 \cos(x_2) + \frac{M_{z_2} R_e g}{K C_{3333}} \left[(C_{1133} + 3C_{2233}) \left(\frac{x_1}{R_e} \right) - \left(\frac{1-\rho^{m+2}}{1-\rho^{2m}} \right) (C_{1133} + (1+m)C_{2233}) \left(\frac{x_1}{R_e} \right)^{m-1} - \left(\frac{1-\rho^{m-2}}{1-\rho^{2m}} \right) \rho^{m+2} (C_{1133} + (1-m)C_{2233}) \left(\frac{x_1}{R_e} \right)^{-m-1} \right] \right\} \cos(x_2) \quad (10.c)$$

$$\tau_{12}^{bend-z_2} = \frac{M_{z_2} R_e g}{K} \left[\left(\frac{x_1}{R_e} \right) - \left(\frac{1-\rho^{m+2}}{1-\rho^{2m}} \right) \left(\frac{x_1}{R_e} \right)^{m-1} - \left(\frac{1-\rho^{m-2}}{1-\rho^{2m}} \right) \rho^{m+2} \left(\frac{x_1}{R_e} \right)^{-m-1} \right] \sin(x_2) \quad (10.d)$$

The shear stress produced by torsional moment M_t is presented in equation (11) at global coordinate z_3 , Lekhnitskii (1981). At Appendix 3 are shown the steps to reach it.

$$\tau_{23}^{torsion} = \frac{M_t}{J} x_1 \quad (11)$$

Where J is the polar second moment of area. To compute the transverse shear effect, the components V_{z_1} and V_{z_2} are summed vectorially. Geometrically, these relations can be written as

$$\varphi = \arctan \left(\frac{V_{z_1}}{V_{z_2}} \right) \quad (12.a)$$

$$V_R = \left(V_{z_1}^2 + V_{z_2}^2 \right)^{\frac{1}{2}} \quad (12.b)$$

The stress generated by the transverse forces V_R in an orthotropic body can be estimated as, Lekhnitskii (1965):

$$\begin{aligned} \tau_{13}^{trans} = & \left(\frac{V_R g}{K C_{3333}} \right) \left(\frac{1}{1-\rho^{2n}} \right) \left\{ \alpha \left[\left(1-\rho^{2n} \right) x_1^2 - R_e^{-n+3} \left(1-\rho^{n+3} \right) x_1^{n-1} \right] - R_i^{n+3} \left(1-\rho^{n-3} \right) x_1^{-n-1} \right] - \\ & - \alpha_p \left[\left(1-\rho^{2n} \right) x_1^m - R_e^{m-n+1} \left(1-\rho^{m+n+1} \right) x_1^{n-1} - R_i^{m+n+1} \left(1-\rho^{-m+n-1} \right) x_1^{-n-1} \right] - \\ & - \alpha_n \left(R_i R_e \right)^{m+2} \left[\left(1-\rho^{2n} \right) x_1^{-m} - R_e^{-m-n+1} \left(1-\rho^{-m+n+1} \right) x_1^{n-1} - R_i^{-m+n+1} \left(1-\rho^{m+n-1} \right) x_1^{-n-1} \right] \right\} \sin(x_2 + \varphi) \end{aligned} \quad (13.a)$$

$$\begin{aligned} \tau_{23}^{trans} = & \left(\frac{V_R g}{K C_{3333}} \right) \left\{ \alpha \left[3x_1^2 - n R_e^{-n+3} \frac{1-\rho^{n+3}}{1-\rho^{2n}} x_1^{n-1} - n R_i^{n+3} \frac{1-\rho^{n-3}}{1-\rho^{2n}} x_1^{-n-1} \right] + \right. \\ & + \left(C_{1133} + C_{2233} - \frac{C_{3333}}{g} \right) x_1^2 - \alpha_p \left[\left(1+m \right) x_1^m - n R_e^{m-n+1} \frac{1-\rho^{m+n+1}}{1-\rho^{2n}} x_1^{n-1} - n R_i^{m+n+1} \frac{1-\rho^{-m+n-1}}{1-\rho^{2n}} x_1^{-n-1} \right] - \\ & - \alpha_n \left(R_i R_e \right)^{m+2} \left[\left(1-m \right) x_1^{-m} - n R_e^{-m-n+1} \frac{1-\rho^{-m+n+1}}{1-\rho^{2n}} x_1^{n-1} - n R_i^{-m+n+1} \frac{1-\rho^{m+n-1}}{1-\rho^{2n}} x_1^{-n-1} \right] - \\ & \left. - R_e^{-m+2} \left(\frac{1-\rho^{m+2}}{1-\rho^{2m}} \right) \left[C_{1133} + \left(1+m \right) C_{2233} \right] x_1^m - R_i^{m+2} \left(\frac{1-\rho^{m-2}}{1-\rho^{2n}} \right) \left[C_{1133} + \left(1-m \right) C_{2233} \right] x_1^{-m} \right\} \cos(x_2 + \varphi) \end{aligned} \quad (13.b)$$

Where n , α , α_p and α_n are constants created to reduce the expressions size and defined at Appendix 1. Note that equations (13.a) and (13.b), for transversally isotropic and isotropic bodies, $C_{2233} = C_{1133}$, and thus $g = 0$, so in turn $\alpha \rightarrow \infty$, the stress distribution takes a simplified form that are presented in equations (14.a) and (14.b).

$$\tau_{13}^{trans_i} = \frac{V_R}{I} \lambda \left[x_1^2 - R_e^{-n+3} \left(\frac{1-\rho^{n+3}}{1-\rho^{2n}} \right) x_1^{n-1} - R_i^{n+3} \left(\frac{1-\rho^{n-3}}{1-\rho^{2n}} \right) x_1^{-n-1} \right] \sin(x_2 + \varphi) \quad (14.a)$$

$$\tau_{23}^{trans_i} = \frac{V_R}{I} \left[-x_1^2 + \lambda \left[3x_1^2 - nR_e^{-n+3} \left(\frac{1-\rho^{n+3}}{1-\rho^{2n}} \right) x_1^{n-1} + nR_i^{n+3} \left(\frac{1-\rho^{n-3}}{1-\rho^{2n}} \right) x_1^{-n-1} \right] \right] \cos(x_2 + \varphi) \quad (14.b)$$

Where I is the second moment of area, λ is a constant created to reduce the expressions size and it is defined in Appendix 1. For this linear elastic study, the stress can be computed using the Superposition Method, Crandall (1978):

$$\tau_{11} = \tau_{11}^{axial} + \tau_{11}^{bend_{z-1}} + \tau_{11}^{bend_{z-2}} \quad (15.a)$$

$$\tau_{22} = \tau_{22}^{axial} + \tau_{22}^{bend_{z-1}} + \tau_{22}^{bend_{z-2}} \quad (15.b)$$

$$\tau_{33} = \tau_{33}^{axial} + \tau_{33}^{bend_{z-1}} + \tau_{33}^{bend_{z-2}} \quad (15.c)$$

$$\tau_{12} = \tau_{12}^{bend_{z-1}} + \tau_{12}^{bend_{z-2}} \quad (15.d)$$

$$\tau_{13} = \tau_{13}^{trans} \quad (15.e)$$

$$\tau_{23} = \tau_{23}^{torsion} + \tau_{23}^{trans} \quad (15.f)$$

For a generic load, the stresses and strains can be analyzed in a 3x3 symmetric matrix. The eigenvalues and eigenvectors of these matrices have a special physical meaning: the eigenvalues are the principal stresses and principal strains and the eigenvectors are their respective angles. Mathematically, the eigenvalues are calculated as

$$\left| \tau_{ij} - \sigma \delta_{ij} \right| = 0 \quad (16)$$

$$\left| e_{ij} - \varepsilon \delta_{ij} \right| = 0 \quad (17)$$

Where σ and ε are the principal stresses and strains and δ_{ij} is the Kronecker delta. Once the eigenvalues are obtained, the eigenvectors can be estimated as

$$\left[\tau_{ij} - \sigma \delta_{ij} \right] \left[l_i \right] = 0 \quad (18)$$

$$\left[e_{ij} - \varepsilon \delta_{ij} \right] \left[m_i \right] = 0 \quad (19)$$

At bone surface, where the plane stress condition takes place, the principal stresses and strains can be also calculated as

$$\sigma_1 = \frac{\tau_{22} + \tau_{33}}{2} + \left[\left(\frac{\tau_{22} - \tau_{33}}{2} \right)^2 + (\tau_{23})^2 \right]^{\frac{1}{2}} \quad (20.a)$$

$$\sigma_2 = 0 \quad (20.b)$$

$$\sigma_3 = \frac{\tau_{22} + \tau_{33}}{2} - \left[\left(\frac{\tau_{22} - \tau_{33}}{2} \right)^2 + (\tau_{23})^2 \right]^{\frac{1}{2}} \quad (20.c)$$

$$\varepsilon_1 = \frac{e_{22} + e_{33}}{2} + \left[\left(\frac{e_{22} - e_{33}}{2} \right)^2 + (e_{23})^2 \right]^{\frac{1}{2}} \quad (20.d)$$

$$\varepsilon_2 = e_{11} \quad (20.e)$$

$$\varepsilon_3 = \frac{e_{22} + e_{33}}{2} - \left[\left(\frac{e_{22} - e_{33}}{2} \right)^2 + (e_{23})^2 \right]^{\frac{1}{2}} \quad (20.f)$$

And the slope of the principal directions on the external surface are

$$\Phi_{stress} = \frac{1}{2} \arctan \left(\frac{2\tau_{23}}{\tau_{33} - \tau_{22}} \right) \quad (21.a)$$

$$\Phi_{strain} = \frac{1}{2} \arctan \left(\frac{2e_{23}}{e_{33} - e_{22}} \right) \quad (21.b)$$

Although the three principal strains are different of zero, there is no distortion caused by shear effect acting on the face perpendicular to the radial direction, thus the direction of the middle principal strain (ε_2) coincides to the radial coordinate (x_1) of Fig. 1.b.

At next section the Finite Element Model is presented, as well as the geometric constants, loads, material constants used to generate the example solved by both models analytical and F.E.

4 FINITE ELEMENT MODEL

A numerical model was developed using the F.E. ANSYS software, through the utilization of a parasolid file of a human femur, that was obtained in a bone file repository, like Biomedtown (2015). The static loading is composed by the joint reaction force and three principal muscles forces, which are positioned at the femur head region, as shown at Figure 2, adapted from Taylor *et al.* (1996):

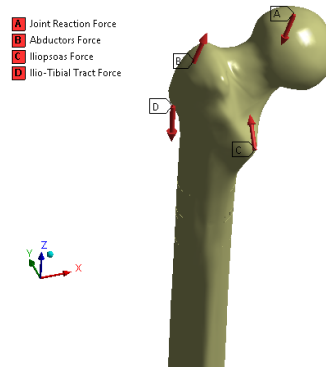


Figure 2: Human femur static loading model.

The bone distal region was fixed to ensure equilibrium requirements. To extract the results, one path, on a medial cross section along the bone external surface was created, as shown in Figure 3.a. The purple arrow indicates the path orientation.

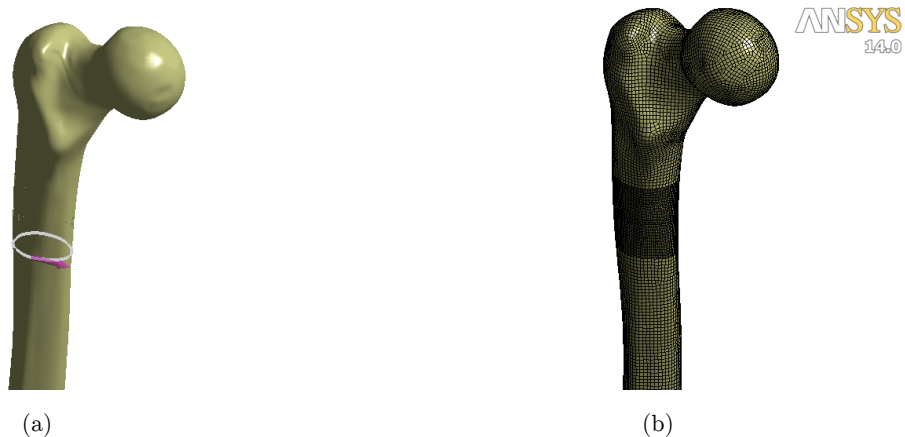


Figure 3: (a) Path created to extract the results and (b) Mesh used on the F.E. simulations..

Figure 3.b shows the mesh used at the human femur bone. At medial section, where the path is located, the mesh was refined to access more accurate results. As the bone has a quite irregular shape, SOLID186 and SOLID187 elements were used, which exhibit a quadratic displacement behavior, and have twenty and ten nodes respectively, see Bathe (2007) and Lee (2012). As can be clear from Figure 3.b, the mesh was separated in three different parts: the medial region where the path was created, the proximal part (above the path) and the distal part (bellow the path).

After a convergence study, in the path region an average element size of 1 mm was applied and in the other parts an average element size of 2 mm were applied. It must be pointed that different from Kenedi and Riagusoff (2015), where tetrahedrons elements were applied on the femur head, in the present study the hexahedron elements was selected. To access a good text about detailed bone mesh, see Ramos and Simões (2006). Table 1 shows the loading forces and geometric constants utilized.

Joint reaction force	P_1 (N)	(-1,062; -130; -2,800)
Abductors force	P_2 (N)	(430; 0; 1,160)
Iliopsoas force	P_3 (N)	(78; 560; 525)
Ilio-Tibial Tract force	P_4 (N)	(0; 0; -1,200)
P_1 point of application	A (mm)	(50.7; -2.7; 133)
P_2 point of application	B (mm)	(-13.5; -6.5; 115)
P_3 point of application	C (mm)	(18.8; -29.3; 58.7)
P_4 point of application	D (mm)	(-24.6; -4.2; 83)
cross section centroid	(mm)	(0.8; 2.4; -25)
R_e (external radius)	(mm)*	15.5
R_i (internal radius)	(mm)*	7.6

Table 1: Loading forces and geometric constants. (* approximate measure).

Note that P_1 , P_2 , P_3 and P_4 are applied, respectively, at points A , B , C and D of Figure 2. The range of cortical human femur bone mechanical properties on the literature is wide, which can be explained by the existing differences between people's bones, as age, diseases, gender, if the bone specimen is fresh or frozen and so on. Table 2 shows the elastic mechanical properties obtained in technical literature, for the cylindrical coordinate system. Three bone material constitutive relations are listed. Only the independent constants are represented (two for isotropic, five for transversally isotropic and nine for orthotropic).

Material Properties	Isotropic ¹	Transversally Isotropic ²	Orthotropic ³
E (GPa)	20	-	-
E_1 (GPa)	-	18.8	12
E_2 (GPa)	-	-	13.4
E_3 (GPa)	-	27.4	20
ν	0.3	-	-
ν_{12}	-	0.312	0.376
ν_{13}	-	0.193	0.222
ν_{23}	-	-	0.234
G_{12} (GPa)	-	-	9.06
G_{13} (GPa)	-	17.42	11.22
G_{23} (GPa)	-	-	12.46

Table 2: Elastic mechanical properties.

¹(Kenedi and Riagusoff, 2015), ²(Yoon and Katz, 1976) and ³(Korsa and Mares, 2012).

The numerical simulation was done with the use of orthotropic mechanical properties. The orthotropic constitutive relationship represents the most general anisotropy case of used by analytical and numerical models in this work. The isotropic and the transversally isotropic relationships can be modeled with the analytical approach proposed by Kenedi and Riagusoff (2015), or be also obtained by the application of the analytical model proposed in this manuscript for $\nu_{32} = \nu_{31}$.

At next section both analytical and F.E. results are presented. The analytical model is used three times, one time with each constitutive relations: the isotropic, the transversally isotropic and the orthotropic. The F.E. model only accesses the results for orthotropic approach.

5 RESULTS

In this section the results of the numerical F.E. model and the analytical model are shown. The models results were presented in terms of principal stresses/strains, as well as, their respective principal angles, which are especially important to check if they can be related with human bone lamellae orientation, as in Petrtýl *et al.* (1996). Figure 4 shows the maximum principal stresses (MPa)/strain (mm/mm) distribution for orthotropic human femur cortical tissue.

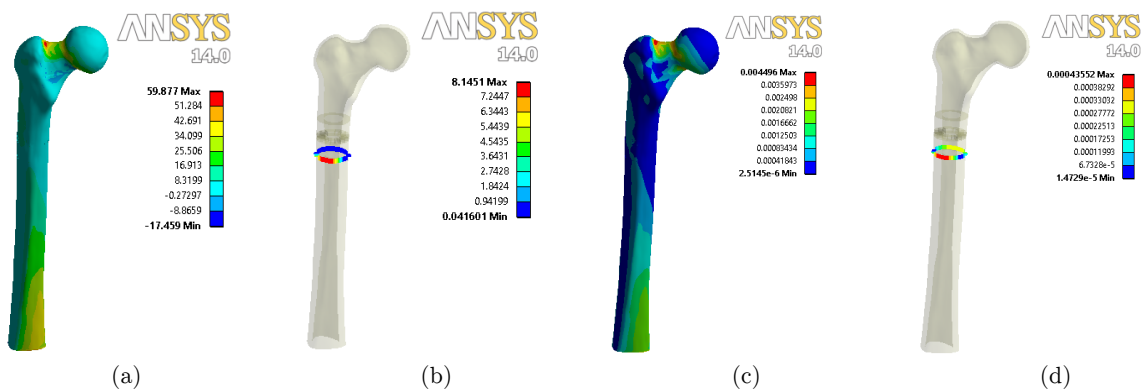


Figure 4: Orthotropic cortical tissue: Maximum principal stresses distribution at: (a) external surface and (b) path; Maximum principal strain distribution at: (c) external surface and (d) path.

Note that using path approach, $0^\circ \leq \theta \leq 360^\circ$, it makes possible to access a more useful results presentation. To validate the analytical model, as well as the hypotheses adopted, the results of the principal stresses and strains for both analytical and numeric models are plotted together at Figure 5. Note that it was utilized the more generic case of anisotropy covered by this work, the orthotropic one, for both analytical and numeric (F.E.) models.

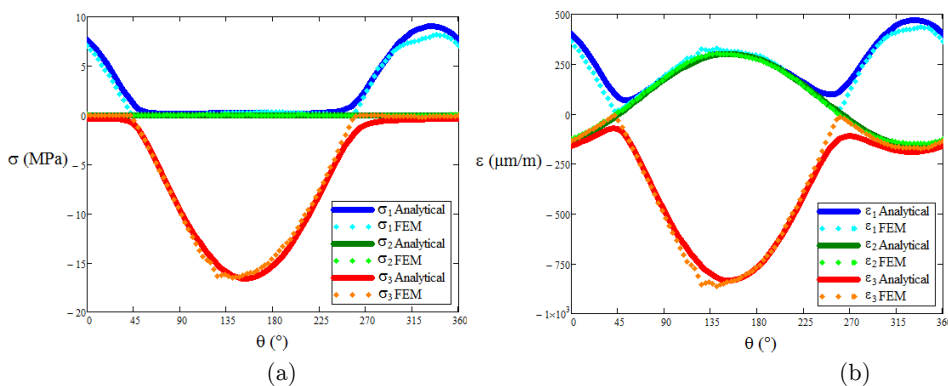


Figure 5: Comparative performance between analytical and numeric models for orthotropic cortical tissue at a medial external bone surface path: (a) principal stresses and (b) principal strains.

Where the σ indexes 1, 2 and 3 refer to the maximum, intermediate and minimum principal stress/strains. Figure 5 shows that the geometry simplification assumed during the analytical approach do not affected significantly the analytical model performance when compared to the numerical approach. Indeed the analytical model performance can be considered quite acceptable.

The elastic mechanical properties presented in Table 2 are used to compare the effect of the level of anisotropy for the principal stress and strains distributions at the medial external bone surface path, respectively at Figures 6 and 7.

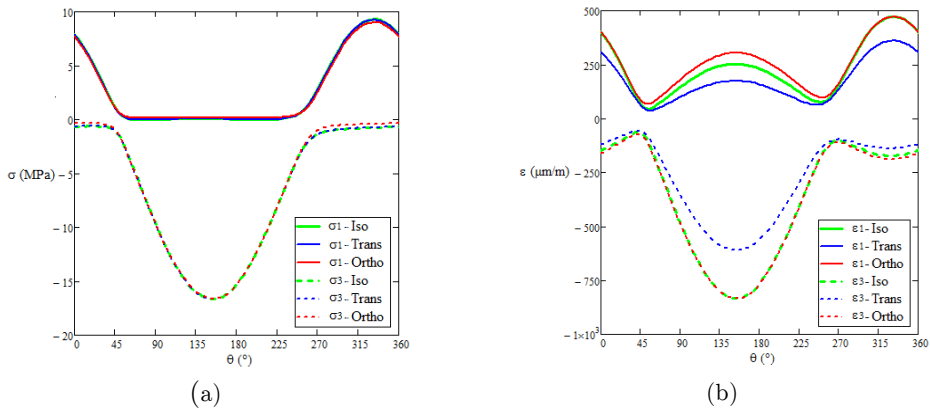


Figure 6: Analytical model results, at a medial external bone surface path, for three different constitutive relations, for principal (a) stresses and (b) strains.

Where Iso, Trans and Ortho represent, respectively, the isotropic, the transversally isotropic and the orthotropic constitutive relations used by the analytical model. Note that the path is along a free external surface, thus the intermediate principal stresses are always null.

At Figure 6, the principal stresses values are almost coincident for all the constitutive relations used by the analytical model, while the principal strains distribution, presents observable differences between curves.

Figures 7.a and 7.b show, respectively, the principal stress and strains angles at the medial bone external surface path for the three constitutive relationships covered in this work.

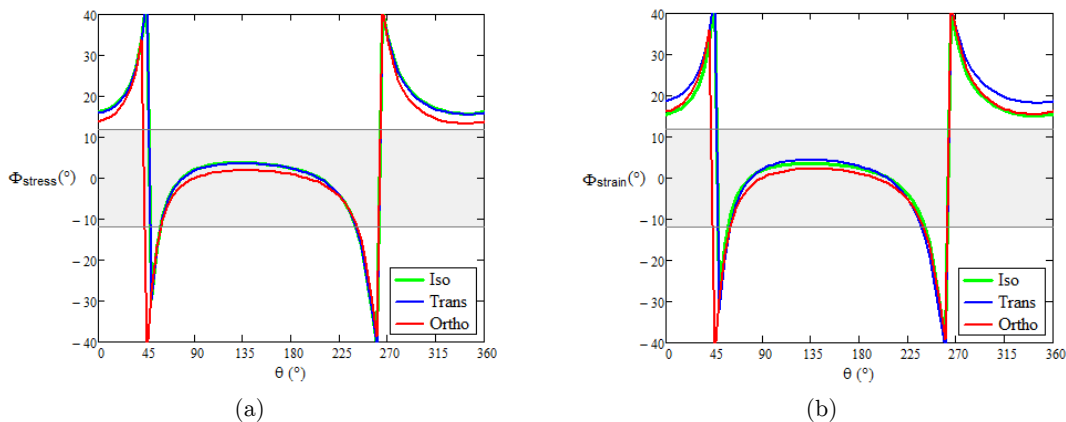


Figure 7: Analytical model results, for three constitutive relations, at a medial external bone surface path, for (a) principal stress angles and (b) principal strain angles.

At Fig. 7 the gray band represents the experimental results related by Petrářl *et al.* (1996) for the experimental slope of bone lamellae range. Also Fig. 7 shows two path angles, around $\theta=45^\circ$ and $\theta=260^\circ$, where there are a vertical asymptotic behavior for both, stress and strain angles. The analytical results shown at Figure 7 reveals that the principal stress angles (Iso) and (Trans) have very similar behaviors, while (Ortho) has a noticeable difference. For principal strain angles, their behaviors are all slightly different.

At Fig. 6 the principal stress and strains are close to zero at path angles $\theta=45^\circ$ and $\theta=260^\circ$, which are where, at Fig. 7, the abrupt changes for both stress and strain angles occur. In these regions there is a remarkable bone lamellae angle change that apparently corresponds to the limit of two opposite helical osteon systems, Petrářl *et al.* (1996).

At next section the results obtained in this section are commented in a more complete way, stressing the principal results obtained in this research.

6 DISCUSSION

As mentioned previously, and commented more detailed by Bayraktar *et al.* (2004), the measurement of bone properties is a difficult task, due to its huge dependence of conservation sample characteristics, irregular geometry, non-homogenous material distribution and anisotropy. Nevertheless, using a macroscopic approach it is possible to model the complex bone mechanical behavior through the utilization of an orthotropic approximation, which can be classified, as proposed at Introduction Section, as a macro paper.

This approach has the advantage of considering the implicit non-uniform density distribution along the thickness, recognizing the elastic mechanical properties variation according to the direction analyzed. See also Cowin (2001).

At Fig. 5 the principal stress and strain analytical and numeric results are compared, at a medial external bone surface path, for orthotropic constitutive relationship. The analytical model results show a good match with numerical model, used here as reference. Fig. 6 compares the analytical model principal stresses/strains results, at a medial external bone surface path, using the three constitutive relationships adopted: orthotropic, transversally isotropic and isotropic. The principal stress results revealed to be quite close, whereas the principal strains showed some perceptible differences.

The proposed model, based in theory of elasticity, see Lekhnitskii (1981), has proven to be consistent to analyze orthotropic materials but rather laborious to be applied. For isotropic material a simpler model, based in solid mechanics, proposed by Kenedi and Riagusoff (2015) can be also used. Nevertheless both models demand the aid of mathematical software, as Mathcad.

The analytical model, using the three constitutive relationships, showed a similar performance for principal stress distribution. For principal strain distributions there were some differences. The principal stress angles (ϕ_{stress}) and the principal strain angles (ϕ_{strain}), inside the path angles $45^\circ \leq \theta \leq 260^\circ$ agrees with the bone lamellae angles range related by Petrářl *et al.* (1996), between -12° and $+12^\circ$. Outside the path angles $45^\circ \leq \theta \leq 260^\circ$, there are no match with bone lamellae angles range. Also, for principal strain angles more differences are present than for principal stress angles between each constitutive relationship.

7 CONCLUSION

The objective of this paper is to propose an analytical model using an anisotropic theory of elasticity, Lekhnitskii (1981), applied to biomechanical tissues, to check if there is a correlation between bone lamellae angles and principal stresses angles. The analytical model describes the principal stress/strain effect of axial and transversal forces, bending and torsion moments in a human femur medial cross section. The presented model was developed for orthotropic materials and can also be applied to transversally isotropic and isotropic materials as particular cases.

A finite element simulation with real femur geometry, submitted to the same load case of analytical model, was carried out to validate the analytical model and their assumptions about the bone irregular geometry. To validate the model, only the orthotropic case was simulated. The path, at a medial external surface of a human femur, was used to obtain the principal stress and strains distribution as well its respective principal angles.

The range of principal stress angles (ϕ_{stress}) and principal strain angles (ϕ_{strain}) values remain inside the shaded area, limited by -12° and $+12^\circ$ angles of Fig. 7, only for path angles θ between 45° and 260° , where the principal stresses has their most negative values. This behavior is compatible with dominant osteonal range angles experimentally obtained by Petrář *et al.* (1996).

Outside the path angles θ between 45° and 260° occurs an abrupt change of both stress and strain angles. In these regions have a remarkable bone lamellae angle change and apparently correspond to the limit of two opposite helical osteon systems, Petrář *et al.* (1996). In this region the principal stress and strain angles reached up to angles that ranged from -40° to $+40^\circ$.

The results show that it is important to take into account significant differences, mainly in principal strains values and principal strain angles, associated to the level of anisotropy of long bones cortical tissues. For a future work, the fatigue evaluation caused by dynamic load will also be taken into account.

References

- Allena, R. and Cluzel, C. (2014). Identification of anisotropic tensile strength of cortical bone using Brazilian test. *Journal of the mechanical behavior of biomedical materials*, 38: 134-142.
- Bathe, K. J. (2006). *Finite Element Procedures*, Prentice Hall.
- Bayraktar H.H., Morgan E.F., Niebur, G.L., Morris, G.E., Wong, E.K., Keaveny, T.M. (2004). Comparison of the elastic and yield properties of human femoral trabecular and cortical bone tissue. *J. Biomech*, 37: 27-35.
- Baumann, A.P., Deuerling, J.M., Rudy, D.J., Niebur, G.L., Roeder, R.K. (2012). The relative influence of apatite crystal orientations and intracortical porosity on the elastic anisotropy of human cortical bone. *J. Biomech*, 45: 2743-2749.
- Carnelli, D., Vena, P., Dao, M., Ortiz, C., & Contro, R. (2013). Orientation and size-dependent mechanical modulation within individual secondary osteons in cortical bone tissue. *Journal of The Royal Society Interface*, 10(81), 20120953.
- Cowin, S.C. (2001). *Bone Mechanics Handbook*, Second Edition, CRC Press.
- Cowin, S.C. and Hart, R.T. (1990). Errors in the orientation of the principal stress axes if bone tissue is modeled as isotropic, *J. Biomech.*, Technical Note, (23), issue 4, pp. 349-352.
- Crandall, S.H., Dahl, N.C. and Lardner, T.J. (1978). *An Introduction to the Mechanics of Solids*, Second Edition with SI units, McGraw Hill International Editions.

- Doblaré, M., García J. M. and Gómez, M. J. (2004). Modeling bone tissue fracture and healing: a review, *Engineering Fracture Mechanics*, (71), pp. 1809-1840.
- https://www.biomedtown.org/biomed_town/LHDL/Reception/datarepository/repositories/BelRepWikiPages/TheStandardizedFemurSolidModel. Accessed 12 August 2015
- Jones, R.M. (1998) *Mechanics of Composite Materials*, Second Edition, Taylor & Francis Editions.
- Kenedi, P.P., Riagusoff, I.I.T.(2015). Stress development at human femur by muscle forces, *J Braz. Soc. Mech. Sci. Eng.*,37(1), pp. 31-43..
- Kenedi, P. P., Vignoli, L. L. (2014). Bone Anisotropy Influence - A Finite Element Analysis. In XXIV Brazilian Congress on Biomedical Engineering–CBEB
- Korsa, R., Mares, T. (2012). Numerical Identification of Orthotropic Coefficients of the Lamella of a Bone's Osteon, *Bulletin of Applied Mechanics*, 8(31), pp. 45-53.
- Krone, R. and Schuster, P. (2006). An Investigation on the Importance of Material Anisotropy in Finite-Element Modeling of the Human Femur, SAE International, 2006-01-0064.
- Lee, H. H. (2012). *Finite Element Simulations with ANSYS Workbench 14*, SDC Publications.
- Lekhnitskii, S.G. (1987). *Anisotropic Plates*, Third Edition, Gordon and Breach Science Publishers.
- Lekhnitskii, S.G. (1981). *Theory of elasticity of an anisotropic body*, Mir.
- Lekhnitskii, S.G. (1965). *Theory of elasticity of an anisotropic elastic body*, Holden-Day Series in Mathematical Physics.
- Petrtyl, M., Herf, J. and Fiala, P. (1996). Spatial Organization of the Haversian Bone in Man, *J. Biomech.*, (29), No. 2, pp. 161-169.
- Raftopoulos, D.D., Qassem, W., (1987). Three-Dimensional Curved Beam Stress Analysis of the Human Femur. *J. Biomed. Eng*, Vol. 9, October, pp. 356-366.
- Ramos A., Simões J.A. (2006). Tetrahedral versus hexahedral finite elements in numerical modelling of the proximal femur. *Med Eng Phys* 28:916–924.
- Rudman K.E., Aspden R.M., Meakin, J.R. (2006). Compression or tension? The stress distribution in the proximal femur. *Biomed. Eng*. 5(12):1-7.
- San Antonio, T., Ciaccia, M., Muller-Karger, C. , Casanova, E. (2012). Orientation of orthotropic material properties in a femur FE model: A method based on the principal stresses directions. *Medical engineering & Physics*, vol. 34, pp.914-919.
- Sih, G.C., Paris, P.C., Irwin, G.R. (1965). On cracks in rectilinearly anisotropic bodies, *International Journal of Fracture Mechanics*, Volume 1, Issue 3, pp 189-203.
- Sokolnikoff, I. S. (1956). *Mathematical Theory of Elasticity*, Second Edition, McGraw-Hill Book Company.
- Taylor, W.R., Roland, E., Ploeg, H., Hertig, D., Klabunde, R., Warner, M.D., Hobato, M.C., Rakotomanana, L. and Clift, S.E. (2002). Determination of orthotropic bone elastic constants using FEA and modal analysis, *J. Biomech.*, (35), pp. 767-773.
- Taylor, M.E., Tanner, K.E., Freeman, M.A.R. and Yettram, A.L. (1996). Stress and strain distribution within the intact femur: compression or bending?, *Med. Eng. Phys.*, vol. 18, pp. 122-131.
- Toridis, T.G., (1969). Stress Analysis of the Femur. *J. Biomech.*, vol. 2, , pp. 163-174.
- Yoon, H.S., Katz, J.L., (1976). Ultrasonic wave propagation in human cortical bone — II. Measurements of elastic properties and microhardness. *J. Biomech.*, 9(7), pp. 459-464.

APPENDICES

Appendix 1

The analytical model constants to transform the original equations proposed by Lekhnitskii (1981) into a more compact form:

$$g = \frac{C_{2233} - C_{1133}}{\beta_{1111} + 2\beta_{1122} + 2\beta_{1212} - 3\beta_{2222}} \quad (\text{I.1})$$

$$h = \frac{C_{2233} - C_{1133}}{\beta_{1111} - \beta_{2222}} \quad (\text{I.2})$$

$$k = \left(\frac{\beta_{1111}}{\beta_{1122}} \right)^{\frac{1}{2}} \quad (\text{I.3})$$

$$K = \frac{\pi R_e^4}{4} (1 - \rho^4) - \frac{\pi R_e^4 g}{C_{3333}} \left[(1 - \rho^4) \frac{C_{1133} + 3C_{2233}}{4} - \frac{(1 - \rho^{m+2})^2}{1 - \rho^{2m}} \left(\frac{C_{1133} + (1+m)C_{2233}}{m+2} \right) - \frac{(1 - \rho^{m-2})^2}{1 - \rho^{2m}} \rho^4 \left(\frac{C_{1133} + (1-m)C_{2233}}{m-2} \right) \right] \quad (\text{I.4})$$

$$I = \left(\frac{\pi R_e^4}{4} \right) (1 - \rho^4) \quad (\text{I.5})$$

$$m = \left(1 + \frac{\beta_{1111} + 2\beta_{1122} + 2\beta_{1212}}{\beta_{2222}} \right)^{\frac{1}{2}} \quad (\text{I.6})$$

$$n = \left(\frac{C_{1313}}{C_{2323}} \right)^{\frac{1}{2}} \quad (\text{I.7})$$

$$T = \pi R_e^2 (1 - \rho^2) + \frac{2\pi h R_e^2}{C_{3333}} \left[\frac{1 - \rho^2}{2} (C_{1133} + C_{2233}) - (1 - \rho^{k+1})^2 \frac{C_{1133} + kC_{2233}}{k+1} - (1 - \rho^{k-1})^2 \rho^2 \frac{C_{1133} - kC_{2233}}{k-1} \right] \quad (\text{I.8})$$

$$\alpha = \frac{1}{2} \frac{C_{3333} \left[\frac{(3C_{2233} - C_{1133} + 6C_{2323})}{g} + (9\beta_{2222} - \beta_{1111}) \right] - 6C_{2323}(C_{1133} + 3C_{2233})}{9C_{2323} - C_{1313}} \quad (\text{I.9})$$

$$\alpha_n = \frac{1}{2} \frac{\left[(1-m)^2 \beta_{2222} - \beta_{1111} \right] C_{3333} - 2(1-m)C_{2323} \left[C_{1133} + (1-m)C_{2233} \right]}{(1-m)^2 C_{2323} - C_{1313}} \left(\frac{R_e^{m-2} - R_i^{m-2}}{R_e^{2m} - R_i^{2m}} \right) \quad (\text{I.10})$$

$$\alpha_p = \frac{1}{2} \frac{\left[(1+m)^2 \beta_{2222} - \beta_{1111} \right] C_{3333} - 2(1+m)C_{2323} \left[C_{1133} + (1+m)C_{2233} \right]}{(1+m)^2 C_{2323} - C_{1313}} \left(\frac{R_e^{m+2} - R_i^{m+2}}{R_e^{2m} - R_i^{2m}} \right) \quad (\text{I.11})$$

$$\beta_{ijkl} = C_{ijkl} - \frac{C_{kl33}C_{ij33}}{C_{3333}} \quad (\text{I.12})$$

$$\lambda = \frac{3C_{2323} - 2C_{1133}}{9C_{2323} - C_{1313}} \quad (\text{I.13})$$

Where β is a reduced compliance matrix.

Appendix 2

The traditional formulation for a prismatic isotropic body subjected to axial load at cross section centroid, for a cross section sufficiently far away for axial force application (Saint-Venant's Principle) considers that the whole body cross section has the same displacement. For a prismatic orthotropic body this is not true. This appendix uses the theory developed by Lekhnitskii (1981) to show this point.

For an orthotropic hollow cylinder, using a combination of the geometrical compatibility and constitutive relations, the following equations can be written, considering the Figure 1.b cylindrical coordinate system:

$$\frac{\partial u_1}{\partial x_1} = C_{1111}\tau_{11} + C_{1122}\tau_{22} + C_{1133}\tau_{33} \quad (\text{II.1.a})$$

$$\frac{1}{x_1} \frac{\partial u_2}{\partial x_2} + \frac{u_1}{x_1} = C_{2211}\tau_{11} + C_{2222}\tau_{22} + C_{2233}\tau_{33} \quad (\text{II.1.b})$$

$$\frac{\partial u_3}{\partial x_3} = C_{3311}\tau_{11} + C_{3322}\tau_{22} + C_{3333}\tau_{33} \quad (\text{II.1.c})$$

$$\frac{1}{2} \left(\frac{1}{x_1} \frac{\partial u_3}{\partial x_2} + \frac{\partial u_2}{\partial x_3} \right) = C_{2323} \tau_{23} \quad (\text{II.1.d})$$

$$\frac{1}{2} \left(\frac{\partial u_1}{\partial x_3} + \frac{\partial u_3}{\partial x_1} \right) = C_{1313} \tau_{13} \quad (\text{II.1.e})$$

$$\frac{1}{2} \left(\frac{1}{x_1} \frac{\partial u_1}{\partial x_2} + \frac{\partial u_2}{\partial x_1} - \frac{u_2}{x_1} \right) = C_{1212} \tau_{12} \quad (\text{II.1.f})$$

If the loading is distributed equally on the cross section, the stresses distribution can be written as:

$$\tau_{11} = 0 \quad (\text{II.2.a})$$

$$\tau_{22} = 0 \quad (\text{II.2.b})$$

$$\tau_{33} = \frac{N}{A} \quad (\text{II.2.c})$$

$$\tau_{23} = 0 \quad (\text{II.2.d})$$

$$\tau_{13} = 0 \quad (\text{II.2.e})$$

$$\tau_{12} = 0 \quad (\text{II.2.f})$$

Substituting equation (II.2) into equation (II.1), generates:

$$\frac{\partial u_1}{\partial x_1} = C_{1133} \frac{N}{A} \quad (\text{II.3.a})$$

$$\frac{1}{x_1} \frac{\partial u_2}{\partial x_2} + \frac{u_1}{x_1} = C_{2233} \frac{N}{A} \quad (\text{II.3.b})$$

$$\frac{\partial u_3}{\partial x_3} = C_{3333} \frac{N}{A} \quad (\text{II.3.c})$$

$$\frac{1}{2} \left(\frac{1}{x_1} \frac{\partial u_3}{\partial x_2} + \frac{\partial u_2}{\partial x_3} \right) = 0 \quad (\text{II.3.d})$$

$$\frac{1}{2} \left(\frac{\partial u_1}{\partial x_3} + \frac{\partial u_3}{\partial x_1} \right) = 0 \quad (\text{II.3.e})$$

$$\frac{1}{2} \left(\frac{1}{x_1} \frac{\partial u_1}{\partial x_2} + \frac{\partial u_2}{\partial x_1} - \frac{u_2}{x_1} \right) = 0 \quad (\text{II.3.f})$$

Integrating the equations (II.3.c), (II.3.d) and (II.3.e):

$$u_1 = C_{1133} \frac{N}{A} x_1 + U_1 \quad (\text{II.4.a})$$

$$u_2 = (C_{2233} - C_{1133}) \frac{N}{A} x_1 x_2 + U_2 \quad (\text{II.4.b})$$

$$u_3 = C_{3333} \frac{N}{A} x_3 + U_3 x_1 \quad (\text{II.4.c})$$

Where U_1 , U_2 and U_3 represent the rigid body motion. As an axial force means an axisymmetric load condition on the cylinder the strains and displacements also must be axisymmetric, thus cannot be a function of the tangential coordinate x_2 , as equation (II.4.b). Because of this, the only condition wherein the load is equally distributed on the cross section is if $(C_{2233} - C_{1133})$ is equal to zero, what implies that ν_{32} is equal to ν_{31} , which characterize that the material must be isotropic or transversally isotropic.

Appendix 3

In this appendix is provided an alternative way of presenting the torsion formulation, originally done by Lekhnitskii (1981). The stress functions presented in (6) of Section 3 are used and considering that the load is axisymmetric:

$$\tau_{11} = \frac{1}{x_1} \frac{\partial F}{\partial x_1} \quad (\text{III.5.a})$$

$$\tau_{22} = \frac{\partial^2 F}{\partial (x_1)^2} \quad (\text{III.5.b})$$

$$\tau_{12} = 0 \quad (\text{III.5.c})$$

$$\tau_{13} = 0 \quad (\text{III.5.d})$$

$$\tau_{23} = -\frac{\partial \psi}{\partial x_1} \quad (\text{III.5.e})$$

τ_{33} is not directly associated with the stress functions but has a relation that can be obtained using the geometrical compatibility, constitutive relation and the identity presents in equation (7). Thus, to obtain the complete solution of the stress distribution in an orthotropic cylinder under torsion, it is necessary find the solution of three different functions: F , ψ and τ_{33} . Applying these results on the geometrical compatibility equation (2) and using the constitutive relation (1),

$$\frac{\partial u_1}{\partial x_1} = C_{1111} \left(\frac{1}{x_1} \frac{\partial F}{\partial x_1} \right) + C_{1122} \left(\frac{\partial^2 F}{\partial (x_1)^2} \right) + C_{1133} \tau_{33} \tag{III.6.a}$$

$$\frac{1}{x_1} \frac{\partial u_2}{\partial x_2} + \frac{u_1}{x_1} = C_{2211} \left(\frac{1}{x_1} \frac{\partial F}{\partial x_1} \right) + C_{2222} \left(\frac{\partial^2 F}{\partial (x_1)^2} \right) + C_{2233} \tau_{33} \tag{III.6.b}$$

$$\frac{\partial u_3}{\partial x_3} = C_{3311} \left(\frac{1}{x_1} \frac{\partial F}{\partial x_1} \right) + C_{3322} \left(\frac{\partial^2 F}{\partial (x_1)^2} \right) + C_{3333} \tau_{33} \tag{III.6.c}$$

$$\frac{1}{2} \left(\frac{1}{x_1} \frac{\partial u_3}{\partial x_2} + \frac{\partial u_2}{\partial x_3} \right) = C_{2323} \left(-\frac{\partial \psi}{\partial x_1} \right) \tag{III.6.d}$$

$$\frac{1}{2} \left(\frac{\partial u_1}{\partial x_3} + \frac{\partial u_3}{\partial x_1} \right) = 0 \tag{III.6.e}$$

$$\frac{1}{2} \left(\frac{1}{x_1} \frac{\partial u_1}{\partial x_2} + \frac{\partial u_2}{\partial x_1} - \frac{u_2}{x_1} \right) = 0 \tag{III.6.f}$$

Remembering that all the derivatives in relation to x_2 must be zero and integrating the equations (III.6.c), (III.6.d) and (III.6.e)

$$u_3 = \int \left[C_{3311} \left(\frac{1}{x_1} \frac{\partial F}{\partial x_1} \right) + C_{3322} \left(\frac{\partial^2 F}{\partial x_1^2} \right) + C_{3333} (\tau_{33}) \right] dx_3 \tag{III.7.a}$$

$$u_2 = \int C_{2323} \left(2 \frac{\partial \psi}{\partial x_1} \right) dx_3 \tag{III.7.b}$$

$$u_1 = \int \left(-\frac{\partial u_3}{\partial x_1} \right) dx_3 \tag{III.7.c}$$

Finding u_1 from equation (III.6.b)

$$u_1 = C_{2211} \left(\frac{\partial F}{\partial x_1} \right) + C_{2222} \left(x_1 \frac{\partial^2 F}{\partial (x_1)^2} \right) + C_{2233} (x_1 \tau_{33}) \tag{III.8}$$

It is possible to solve equations (III.7.a) and (III.7.c) to find u_1 :

$$\begin{aligned} & C_{2211} \left(\frac{\partial F}{\partial x_1} \right) + C_{2222} \left(x_1 \frac{\partial^2 F}{\partial (x_1)^2} \right) + C_{2233} (x_1 \tau_{33}) = \\ & = - \int \left[\int C_{3311} \left(-\frac{1}{x_1^2} \frac{\partial F}{\partial x_1} + \frac{1}{x_1} \frac{\partial^2 F}{\partial x_1^2} \right) + C_{3322} \left(\frac{\partial^3 F}{\partial x_1^3} \right) + C_{3333} \left(\frac{\partial \tau_{33}}{\partial x_1} \right) dx_3 \right] dx_3 \end{aligned} \quad (\text{III.9})$$

From equation (III.9), it is possible to conclude that the only solution for this equation is when the right side of the equation is equal to zero because the left side cannot be a function of x_3 , then $e_{33} = 0$, which results that the right side is also null, or $e_{22} = 0$. Using the identity presented in equation (7) and some algebraic manipulations lead to:

$$\frac{\partial e_{11}}{\partial x_1} = 2 \frac{\partial e_{22}}{\partial x_1} + x_1 \frac{\partial^2 e_{22}}{\partial x_1^2} \quad (\text{III.10})$$

As $e_{22} = 0$, as discussed above, $\partial e_{11} / \partial x_1 = 0$ to follow the identity introduced by equation (7), which is represented in a simplified form at equation (III.10). It is possible to realize the substitution of the strain e_{11} , obtained in (III.6.a), into (III.10) that the only possible solution is $F = \tau_{33} = 0$. Replacing (III.7.b) in (III.6.f)

$$2C_{2323} \int \left(\frac{\partial^2 \psi}{\partial x_1^2} - \frac{1}{x_1} \frac{\partial \psi}{\partial x_1} \right) dx_3 = 0 \quad (\text{III.11})$$

Where the solution of this differential equation is

$$\psi = K_1 (x_1)^2 + K_2 \psi \quad (\text{III.12})$$

Note that stress is proportional to $\frac{\partial \psi}{\partial x_1}$, thus only one boundary condition is necessary, the value of K_2 is not necessary. Using the equilibrium condition

$$\int \tau_{23} x_1 dA = M_t \quad (\text{III.13})$$

Thus

$$K_1 = \frac{M_t}{J} \quad (\text{III.14})$$

Where $J = \frac{\pi}{2} (R_e^4 - R_i^4)$ is polar second moment of area, what means that the stress distribution is equal to that one for isotropic cylinders.

This deduction developed in this appendix shows that the stress distribution for orthotropic cylinder under torsion is equal to the stress distribution of an isotropic cylinder.